*Desalination and Water Treatment*
www.deswater.com

doi: 10.5004/dwt.2020.25347

184 (2020) 282–291
April

# Phosphorous removal by nanoscale zero-valent iron (nZVI) and chitosan-coated nZVI (CS-nZVI)

A. Shanableh[a,b], N. Darwish[a,*], S. Bhattacharjee[c], G. Al-Khayyat[b], M. Khalil[a], M. Mousa[a], A. Tayara[a,b], M. Al-Samarai[c]

[a]*Research Institute of Sciences and Engineering, University of Sharjah, Sharjah, United Arab Emirates, Tel. +971-6-5166332; emails: ndarwish@sharjah.ac.ae (N. Darwish), shanableh@sharjah.ac.ae (A. Shanableh), mkhalil@sharjah.ac.ae (M. Khalil), mmousa2@sharjah.ac.ae (M. Mousa), u17200708@sharjah.ac.ae (A. Tayara)*
[b]*Department of Civil & Environmental Engineering, University of Sharjah, Sharjah, United Arab Emirates, email: u15100751@sharjah.ac.ae (Al.-Khayyat)*
[c]*Sharjah Research Academy, Sharjah, United Arab Emirates, shorjo.b@sra.ae (S. Bhattacharjee), samarai@sharjah.ac.ae (M. Al.-Samarai)*

*Received 10 July 2019; Accepted 12 December 2019*

**ABSTRACT**

In this study, nanoscale zero-valent iron (nZVI) and chitosan-coated nZVI (CS-nZVI) adsorbents were synthesized and used for phosphorus removal from an aqueous solution under oxic conditions. The characteristics of the nZVI particles were assessed using scanning electron microscopy, X-ray diffraction, Brunauer–Emmett–Teller surface area and atomic force microscopy. Results showed smooth and spherical $Fe^0$ particles with a size in the range of 74–186 nm for the nZVI compared to a range of 117–200 nm for the CS-nZVI. Adsorption and kinetic experiments were conducted to evaluate phosphorus removal under varying conditions of initial pH (pH 5 and 7) and presence of interfering anions (a mixture of $PO_4^{3-}$, $Cl^-$, $SO_4^{2-}$, $NO_3^-$). Overall, phosphorus adsorption by both nZVI and CS-nZVI was well represented by both, Freundlich and Langmuir isotherms, with the Langmuir isotherm providing a better data fit ($0.950 \le R^2 \le 0.996$). The phosphorus adsorption capacity of nZVI reached 437 mg/g at pH 5 and 169 mg/g at pH 7. CS-nZVI demonstrated drastically lower phosphorus removal capacities than nZVI (289 mg/g at pH 5 and 152 mg/g at pH 7). The adsorption kinetics of both adsorbents, nZVI and CS-nZVI, were well represented by the pseudo-second-order kinetic model ($0.899 \le R^2 \le 0.999$), with the initial adsorption rate being higher at pH 5 than at pH 7. Interfering anions did not significantly alter the phosphorus removal rate or capacity of nZVI particles at pH 5 and pH 7.

*Keywords:* Adsorption; Adsorption capacity; Adsorption kinetics; Zero-valent iron nanoparticles; Chitosan-coated zero-valent iron nanoparticles; Phosphorous removal; Water treatment

## 1. Introduction

Phosphorous is used in a number of industrial and household applications such as food processing, detergents, semi-conductors, flame retardants and fertilizers [1]. Phosphorus is a critical element in aquatic ecosystems and is often considered the limiting nutrient in eutrophication. Reduction of phosphorus discharges from municipal, industrial and agricultural sources is essential to protect water bodies, and technologies to effectively remove phosphorus from aqueous discharges are in demand.

Phosphorus removal can be achieved using physical, chemical and biological processes. Adsorption is a relatively

* Corresponding author.

simple and economical water treatment technique [2] that can effectively be implemented for phosphorus removal. Researchers [3–11] reported adsorption capacities in the range of 1–82 mg P/g for a variety of phosphorus adsorbents, including Al- and Fe-modified bentonites, bio-char, zeolites, titanium oxide particles, anthracite, shale, and other materials. Moharami and Jalali [7] compared the performance of bentonite, calcite, kaolinite, and zeolite (modified with $Fe^{3+}$, $Ca^{2+}$, and $Na^{+}$) as phosphorus adsorbents and reported maximum sorption by $Fe^{3+}$ adsorbents as follow: 1.31 mg/g (bentonite), 1.97 mg/g (calcite), 1.31 mg/g (kaolinite) and 1.58 mg/g (zeolite). Jiang et al. [5] used sponge iron for phosphate removal and observed removal capacity of 1.1 mg/g. Comparatively, higher removal capacities were observed for mesoporous $TiO_2$ [12], which demonstrated phosphorus removals up to 50 mg/g. Furthermore, maximum adsorption capacity of 57–82 mg/g was reported for different types of magnesium biochars [3].

In recent years, nanomaterials, such as nanoscale zero-valent iron (nZVI), have emerged as promising materials for pollution control applications. The nZVI particles were effectively used to remove contaminants such as heavy metals, nutrients and dyes through surface adsorption and precipitation mechanisms [13–17]. However, only a few studies investigating the removal of phosphorus by nZVI have been reported. For instance, Wen et al. [18] demonstrated that nZVI could be used as an effective adsorbent for the removal of phosphate from an aqueous solution, achieving a maximum phosphate adsorption capacity of 245 mg/g. The study [16] also demonstrated an inverse relationship between adsorption capacity and pH wherein the removal of phosphate decreased with increasing pH. Removal of phosphorus from an aqueous solution was attributed to adsorption as well as chemical precipitation [18,19], evidenced by the X-ray diffraction (XRD) patterns of nZVI after exposure to phosphorus, which indicated the formation of crystalline vivianite ($Fe_3(PO_4)_2{\cdot}8H_2O$) [19].

Another factor that may influence the removal capacity of phosphorus by nZVI is the presence of surface coatings. nZVI particles are often coated with surface modifiers such as organic polymers and long-chain organic molecules [20] to improve their colloidal stability against aggregation. Chitosan is a non-toxic polyelectrolyte derived from seafood waste that can be easily degraded by different microorganisms and enzymes. Recently, chitosan and its modified forms have been used in environmental remediation applications for removal of heavy metals and organic pollutants, and have also shown potential as stabilizers and supports for nanomaterials. For instance, Geng et al. [21] have investigated the use of chitosan stabilized-$Fe^0$ nanoparticles to enhance the adsorption of hexavalent chromium from an aqueous solution and observed removal capacities of 145–148 mg/g for CS-Fe compared to 111.7 mg/g for nZVI only. However, studies using chitosan-coated nZVI (CS-nZVI) for phosphorus removal were not available.

In this study, nZVI, and CS-nZVI adsorbents were synthesized characterized then used for phosphorus removal from an aqueous solution under oxic conditions. The study involved assessing and comparing the adsorption capacities and kinetics of the two adsorbents at pH 5 and 7.

## 2. Materials and methods

### 2.1. Preparation of nZVI and CS-nZVI Particles

nZVI was prepared by reducing nZVI particles Fe(II) using potassium borohydride ($KBH_4$). The concentration of $KBH_4$ was six times that of Fe(II) in order to ensure complete reduction [22]. The preparation procedure was as follows: 0.8934°g of Fe(II) sulfate heptahydrate ($FeSO_4{\cdot}7H_2O$) was dissolved in 30 mL deoxygenated water. In addition, 2 mL of ethanol was added to the solution, which was stirred for 5 min under an inert atmosphere of nitrogen. Thereafter, 15 mL of an aqueous solution containing 1.0401 g of potassium borohydride ($KBH_4$) was added dropwise to the mixture using a syringe, which resulted in the formation of black nZVI particles and evolution of hydrogen gas, $H_2$. The resulting solution was stirred for 90 min to complete the reduction of the iron. Finally, 3 ml of ethanol was added to the solution 5 min prior to switching off the stirrer. The resulting nZVI particles were washed by deoxygenated water three times to remove excess chemicals followed by three washes using ethanol. The synthesized nZVI was then kept in ethanol ($CH_3CH_2OH$) at room temperature for characterization.

A similar procedure was followed to prepare the CS-nZVI particles where medium molecular weight chitosan (Sigma-Aldrich, United States) was dissolved in 0.05 M acetic acid ($CH_3COOH$) to prepare a 0.5% by weight solution. The chitosan mixture was stirred for 7 h and was filtered through a 0.22 μm filter to remove any precipitate or undissolved particles. To prepare the CS-nZVI, 3 mL of the 0.5% chitosan solution was added to the Fe(II) sulfate heptahydrate solution, providing a CS:Fe mass ratio of 0.05:1 (0.015 g CS to 0.328 g Fe), and stirred for 30 min under nitrogen gas prior to adding the potassium borohydride ($KBH_4$) solution.

### 2.2. Phosphorus adsorption kinetics

The phosphorus adsorption kinetic experiments were conducted using both nZVI and CS-nZVI at pH 5 and pH 7. At pH 5, an adsorbent dosage of 7.3 mg nZVI was added to 30 mL solution containing 125 mg P/L, whereas at pH 7, an adsorbent dosage of 6.7 mg was mixed with 20 mL solution containing 100 mg P/L. For CS-nZVI, 4.6 mg was added to 20 mL, 125 mg P/L solution at pH 5 and 6.0 mg CS-nZVI was added to 20 mL, 100 mg P/L solution at pH 7. Small variations in quantities of nZVI and CS-nZVI produced during batch synthesis affected the use of quantities of adsorbents. Two other sets of experiments were conducted to assess the impact of the presence of chlorides, nitrates and sulfates on nZVI phosphorous removal kinetics at pH 5 and pH 7. The experiments were conducted in 50 mL flasks each filled with 5.5 mg nZVI mixed in 30 mL anion solutions containing approximately 100 mg/L of each of the following anions: ($PO_4$–P, $Cl^-$, $SO_4^{2-}$ and $NO_3^-$). In conducting the kinetics experiments, a number of flasks were prepared and the experiments were stopped in the different flasks at various predetermined mixing times to measure residual phosphorus concentrations at different reaction times.

The experiments were conducted at 25°C and the contents of the flasks were mixed using a shaker (Model

SMX 1200) oscillating at 200 rpm. The initial pH was adjusted as needed using either sodium hydroxide or acetic acid solutions. Following adsorption, the contents of each flask were immediately centrifuged at 5,000 rpm to separate the adsorbent from the solution, and the residual phosphorus concentrations were measured. The initial phosphorus adsorption capacity ($q_t$) at a time ($t$) was calculated using the following equation:

$$q_t\left(\frac{\text{mg}}{\text{g}}\right)=\frac{\left(C_i-C_t\right)\times V}{W} \tag{1}$$

where $C_i$ (mg/L) is the initial concentration of phosphorus in solution, $C_t$ (mg/L) is the concentration of phosphorus in solution at time $t$, $V$ is the volume of the solution (L), and $W$ is the mass of dry adsorbent (g) used for adsorption.

### 2.3. Adsorption experiments

Two sets of phosphorus adsorption experiments were conducted at pH 5 and pH 7 to assess the adsorption capacity of nZVI. The experiments were conducted in 50 mL conical Erlenmeyer flasks, each filled with 30 mL phosphorus solution with concentrations in the range of 0 to 175 mg P/L, with 6.7–7.3 mg nZVI added to each flask. Two additional sets of experiments were conducted at pH 5 and pH 7 to assess the adsorption capacity of CS-nZVI. The experiments were conducted in 50 mL conical Erlenmeyer flasks, each filled with 20 mL phosphorus solutions to which 4.6–6 mg CS-nZVI was added.

Additional experiments were conducted at pH 5 and pH 7 using synthetic solutions containing a mixture of anions (i.e., phosphate, sulphate, chloride, and nitrate) to assess the impact of other anions on phosphorus removal. Various dilutions of a stock solution containing 150 mg/L of each anion ($PO_4$–P, $Cl^-$, $SO_4^{2-}$ and $NO_3^-$) were used. The experiments were conducted in 50 mL flasks filled with 30 mL mixed anion solutions and 5.5 mg nZVI.

The adsorption experiments were conducted at 25°C and the contents of the flasks were mixed for one hour using a shaker (Model SMX 1200) oscillating at 200 rpm. The equilibrium time of one hour was selected based on the results of the kinetic experiments. The equilibrium phosphorus adsorption capacity, $q_e$, was calculated based on the difference between the initial phosphorus concentration and the equilibrium phosphorus concentration in solution following one hour of mixing ($C_f$) as follows:

$$q_e\left(\frac{\text{mg}}{\text{g}}\right)=\frac{\left(C_i-C_f\right)\times V}{W} \tag{2}$$

## 3. Result and discussion

### 3.1. Characterization of ZVI particles

The morphology and structural heterogeneity of the surface of the iron nanoparticles were examined using a scanning electron microscopy (SEM) (TESCAN VEGA XM variable pressure SEM, Czech Republic) at SEM HV: 30 kV and SEM MAG: 125 Kx. The SEM images in Figs. 1 and 2 show that both the nZVI and CS-nZVI particles appeared smooth and spherical. The particles assumed chain-like aggregates, possibly due to their inherent magnetic properties as well as sample preparation procedure, which required drying of the nanoparticles [19]. The estimated nominal size of the nZVI particles was in the range of 74–186 nm compared to 117–200 nm for the CS-nZVI.

The XRD analysis was conducted using Bruker D8 (United States) Advance XRD (maximum voltage: 40 kV, maximum current: 40 mA and X-ray source: Cu). Fig. 3 clearly shows ZVI ($Fe^0$) at $2\theta = 45°$, with some iron oxide at $2\theta = 35°$ (i.e., magnetite $Fe_3O_4$ or maghemite $Fe_2O_3$, [18]). The oxides may be generated during sample synthesis or preparation for XRD measurement. The baseline of the XRD for CS-nZVI is noisier and the ZVI and iron oxide peaks are less defined than those for nZVI indicating the impact of chitosan on the nZVI particles. Furthermore, the low-intensity peak at $2\theta = 17°$ can be attributed to the presence of chitosan [23].

Moreover, nitrogen adsorption analysis using Autosorb iQ from Quantachrome (United States) was used to determine the Brunauer–Emmett–Teller surface area for the nZVI, which was found to be 14.66 $m^2/g$.

The surface topography or roughness of the ZVI nanoparticles was evaluated using atomic force microscopy (FlexAxiom with C3000 controller, Nanosurf AG, Switzerland). Fig. 4 presents 2D and 3D images of the surface structures, indicating the surface topography or roughness of the nZVI material. The root mean square roughness, Rrms, was measured to be 13.76 nm for the nZVI particles, which agrees with earlier reported values [17].

### 3.2. Phosphorus removal kinetics

The kinetics of phosphorus removal by nZVI were investigated in the presence and absence of chitosan surface coating, and interfering anions, at two initial pH levels (pH 5 and 7) as shown in Figs. 5–7. Overall, the kinetic results show that adsorption was rapid during the first 10–20 min, reaching about 80% of the maximum removal capacity, then slowed down in the following 10 min and then stabilized between 30–60 min. The observed adsorption rate trends were consistent with earlier reported results for various adsorbents [24].

The kinetic parameters were estimated using both pseudo-first-order and pseudo-second-order kinetic models. The two-rate models are presented in Eqs. (3) and (4), with their linear forms presented in Eqs. (5) and (6). The initial pseudo-second-order adsorption rate can be approximated by Eq. (6) for t values that approach zero (i.e., $q_t$ approaches zero and $q_e$–$q_t$ approaches $q_e$ [8].

$$\frac{dq_t}{dt}=k_1\left(q_e-q_t\right) \tag{3}$$

$$\frac{dq_t}{dt}=k_2\left(q_e-q_t\right)^2 \tag{4}$$

$$\log\left(q_e-q_t\right)=\log\left(q_e\right)-k_1t \tag{5}$$

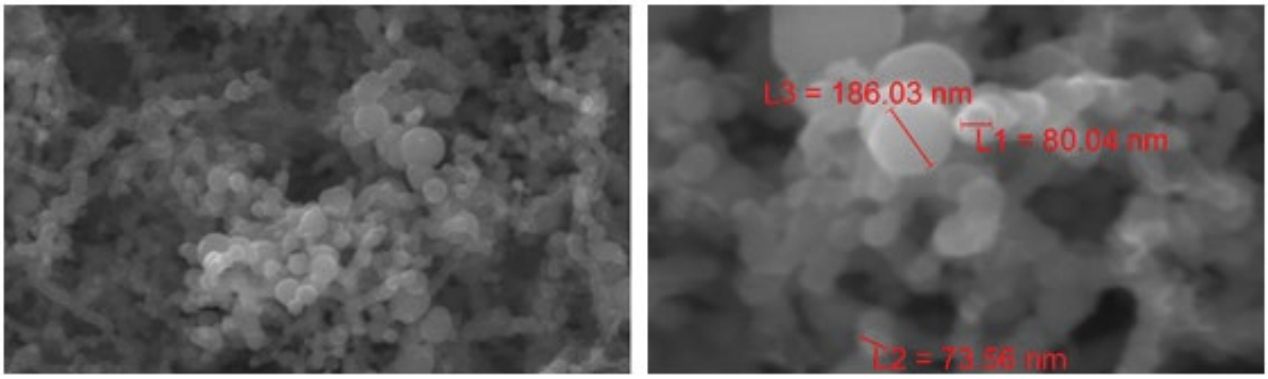


Fig. 1. Scanning electron micrographs of the nZVI Particles.

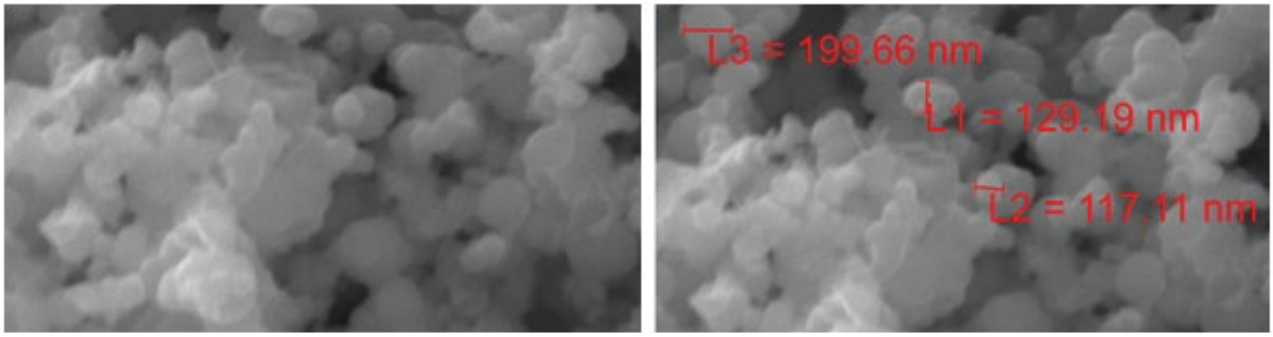


Fig. 2. Scanning electron micrographs of the CS-nZVI.

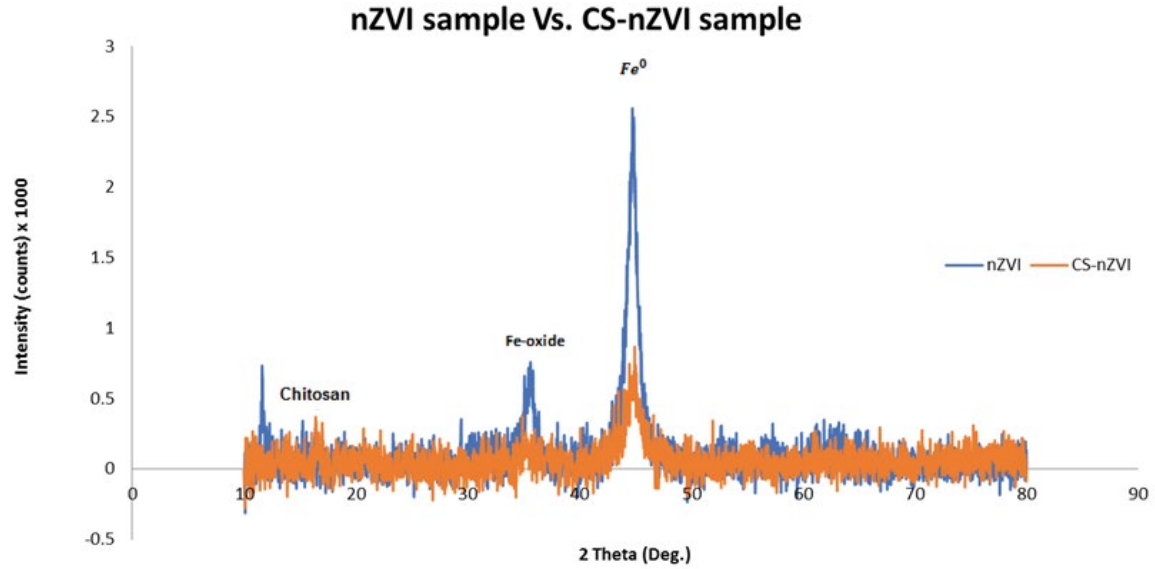


Fig. 3. XRD results for nZVI and CS-nZVI showing $Fe^0$ peaks.

$$\frac{t}{q_t} = \frac{1}{k_2 q_e^2} + \frac{1}{q_e} t \quad (6)$$

$$\frac{dq_t}{dt} = k_2 q_e^2 \quad (7)$$

where $q_e$ is the equilibrium phosphorus adsorption capacity (mg/g), $q_t$ is phosphorus adsorption capacity at time t (min), $k_1$ is the pseudo-first-order rate constant ($min^{-1}$), and $k_2$ is the pseudo-second-order rate constant in (g/mg/min) [8].

The results demonstrated that the pseudo-second-order kinetic model better represented the phosphorus removal

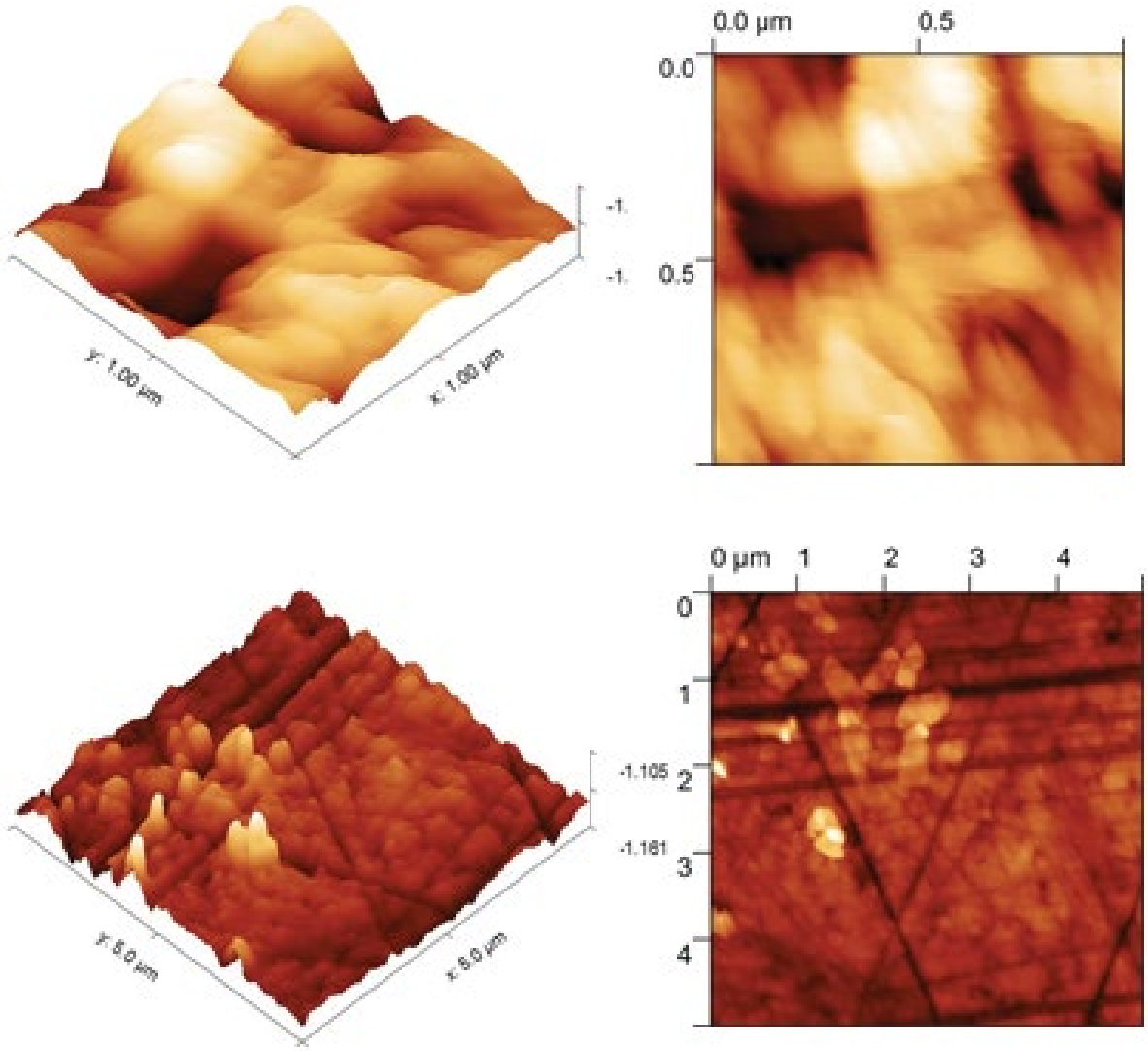


Fig. 4. 3-D and 2-D image profiles of the prepared nZVI particles (Tip used: No-Contact Long Cantilever Reflex Coating (NCLR), scanning speed: 1s per line scanning points: 256 per line).

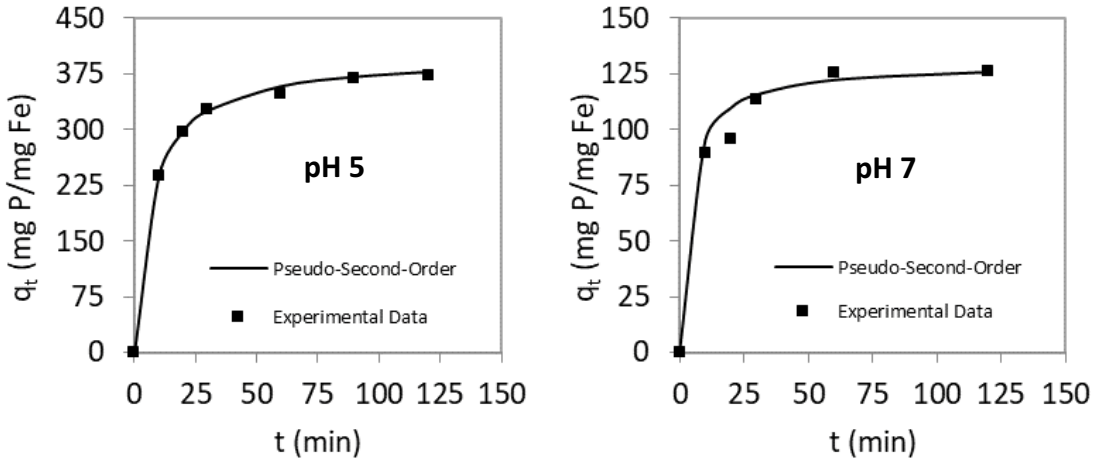


Fig. 5. Pseudo-second-order kinetics of phosphorus adsorption onto nZVI particles at pH 5 and pH 7.

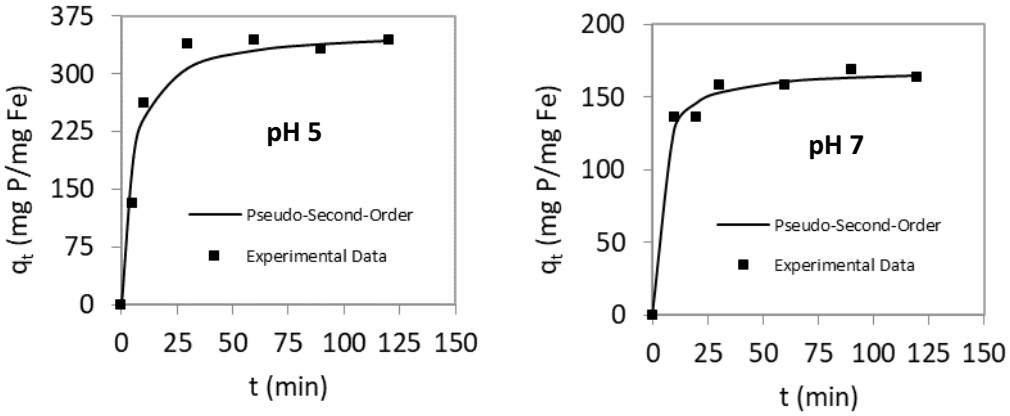


Fig. 6. Pseudo-second-order kinetics of phosphorus adsorption onto nZVI particles at pH 5 and pH 7 from synthetic solutions containing a mixture of anions ($PO_4^{3-}$, $Cl^-$, $SO_4^{2-}$, $NO_3^-$).

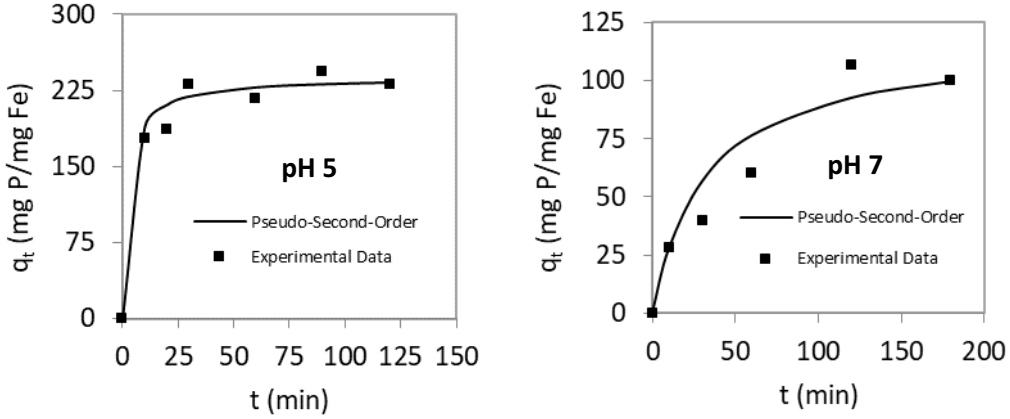


Fig. 7. Pseudo-second-order kinetics of phosphorus adsorption onto CS-nZVI particles at pH 5 and pH 7.

kinetics, with correlation coefficient ($R^2$) values in the range from 0.899 to 0.999. In comparison, the pseudo-first-order kinetic model provided lower $R^2$ values in the range from 0.662 to 0.970. The kinetic parameters obtained for both pseudo-first-order and pseudo-second-order model are presented in Table 1. The data in Table 1 show that the phosphate adsorption capacities (i.e., $q_e$ values) were in the range of 130–400 mg P/g nZVI and 118–238 mg P/g CS-ZVI, indicating that the chitosan reduced the maximum adsorption capacity of nZVI. The removal of phosphorus by nZVI (in the absence of surface coating or interfering ions) was different at the two initial pH levels investigated. At pH 5, a $q_e$ of 400 mg/g was achieved, while at pH 7, $q_e$ was significantly lower at 130 mg/g. A comparison of the initial pseudo-second-order adsorption rate ($dq_i/dt = k_2 \times q_e^2$) shows that phosphorus removal was nearly twice as fast at pH 5 (64 mg $g^{-1}$ $min^{-1}$) compared pH 7 (36.0 mg $g^{-1}$ $min^{-1}$). Overall, the lower initial pH favored phosphorus removal by nZVI achieving higher extent of removal at a faster rate.

A recent study by Nagoya et al. [25] on the mechanisms of phosphate removal by granular ZVI suggested the involvement of both precipitation and adsorption processes. Precipitation occurs due to the corrosion of $Fe^0$ and subsequent release of $Fe^{2+}$ resulting in the formation of $FePO_4$ and $Fe_3(PO_4)_2$ in solution. The adsorption process is dependent on the particle surface charge, wherein at pH ≤ the isoelectric point of nZVI (isoelectric point for nZVI is typically between 6 to 9), the sorption of anionic phosphate is favored onto the positive charge nZVI surface. The authors showed that at pH > 5, adsorption contributed more significantly to the removal of phosphate compared to precipitation. However, the authors also reported a higher phosphate removal by granular ZVI at pH 7 compared to pH 4.5. The discrepancy between the study could be related to the pH control employed by the authors throughout the duration of experiments, whereas in our study no pH control was carried out. Wu et al. [19] and Wen et al. [18] also reported that the removal of phosphorus using nZVI decreased at higher pH, attributing it to the isoelectric point effect. Other factors such as a change in dominant phosphate species in solution (i.e., $H_2PO_4^-$ is dominant at pH 5 while at pH 7 both $H_2PO_4^-$- and $HPO_4^{2-}$- are almost equally dominant) may also influence the adsorption efficiency.

The pseudo-second-order phosphorus adsorption kinetic trends in the presence of interfering ions ($Cl^-$, $SO_4^{2-}$, $NO_3^-$) were also evaluated for nZVI. Because CS-nZVI showed lower phosphate adsorption capacities compared to nZVI,

Table 1
Parameters for pseudo-first-order and pseudo-second-order kinetics

| Type | Solution | pH | $C_i$ (mg/L) | $q_{e,\mathrm{Exp}}$ (mg/g)* | Pseudo-first-order | | | Pseudo-second-order | | | |
|---|---|---|---|---|---|---|---|---|---|---|---|
| | | | | | $k_1$ ($\mathrm{min^{-1}}$) | $q_{e,\mathrm{cal}}$ (mg/g) | $R^2$ | $k_2$ (g/mg min) | $q_{e,\mathrm{cal}}$ (mg/g) | $k_2$ (mg/g min) | $R^2$ |
| nZVI | $PO_4^{3-}$, solution | 5 | 125 | 374 | 0.0191 | 252.3 | 0.970 | 0.0004 | 400 | 64 | 0.999 |
| | | 7 | 100 | 125 | 0.0302 | 107.1 | 0.983 | 0.0021 | 130 | 36.0 | 0.997 |
| CS-nZVI | $PO_4^{3-}$, | 5 | 125 | 230 | 0.0408 | 129.4 | 0.837 | 0.00165 | 238 | 93.5 | 0.995 |
| | solution | 7 | 100 | 90 | 0.012 | 80.7 | 0.688 | 0.0026 | 118 | 36.2 | 0.899 |
| nZVI | Mixture of, | 5 | 100 | 344 | 0.0184 | 116.6 | 0.662 | 0.0006 | 357 | 76.5 | 0.997 |
| | $PO_4^{3-}$, $Cl^-$, | 7 | 100 | 164 | 0.0158 | 55.7 | 0.824 | 0.00185 | 169 | 52.8 | 0.998 |
| | $SO_4^{2-}$, $NO_3^-$ | | | | | | | | | | |

*Experimentally determined

the effect of interfering anions on CS-nZVI was not probed further.

The kinetics trends for phosphate removal by nZVI observed at pH 5 and pH 7 in the presence of a mixture of interfering anions ($Cl^-$, $SO_4^{2-}$, $NO_3^-$) were similar to the trends observed in solutions without the anions. From Table 1 we observe that a higher $q_e$ = 357 mg/g was attained at pH 5 compared to $q_e$ = 169 mg/g at pH 7. The initial rates were also higher at pH 5 (76.5 mg $g^{-1}$ $min^{-1}$) compared to pH 7 (52.8 mg $g^{-1}$ $min^{-1}$). In a previous study by Almeelbi and Bezbaruah [24], the authors reported slight improvements (3%) in phosphate removal by nZVI in the presence of $NO_3^-$, while presence of $SO_4^{2-}$ resulted in a decrease of 24% in phosphate removal. The data presented graphically by the authors also suggested an increase in phosphate removal rates in the presence of $NO_3^-$ while a decrease in rates was observed in the presence of $SO_4^{2-}$, compared to that in deionized water.

In this study, upon comparing the kinetic parameters in the presence and absence of interfering anion mixture, we observe increases in the phosphate removal rates in the presence of anions at both pH 5 and 7. For instance, at pH 5, initial phosphate removal rate was 64 mg $g^{-1}$ $min^{-1}$ in the absence of anions whereas it was 76.5 mg $g^{-1}$ $min^{-1}$ in the presence of anions. However, the $q_e$ showed an appreciable change only at pH 7 (increased from 130 mg/g in the absence of anions, to 169 mg/g in the presence of anions). The differences could be due to mixed effects arising from corrosion and nZVI surface pitting due to $Cl^-$ and formation of iron oxides sorption sites due to reaction of nZVI with $NO_3^-$ [24,26]. However, further studies are needed to elucidate the exact mechanisms for the observed effects.

Table 1 also highlights the kinetics of chitosan-coated nZVI (CS-nZVI). The kinetics of phosphate removal by nZVI and CS-nZVI were similar at pH 7, with $q_e$ = 130 mg/g and initial rate $dq_t/dt = k_2 \times q_e^2$ = 36.0 mg $g^{-1}$ $min^{-1}$ for nZVI, and $q_e$ = 118 mg/g and initial rate = 36.2 mg $g^{-1}$ $min^{-1}$ for CS-nZVI. This could be due to the poorer solubility of chitosan in non-acidic solutions (pH ≥ 7) which may cause precipitation of the coating in solution resulting in poorer surface coverage. This makes the kinetic behavior of CS-nZVI and nZVI similar at pH 7. However, a significant reduction in the adsorption capacity of CS-nZVI was observed at pH 5 with $q_e$ = 238 mg/g compared to nZVI which attained a $q_e$ = 400 mg/g. In contrast, the initial rate was higher for CS-nZVI at pH 5 = 93.5 mg $g^{-1}$ $min^{-1}$ compared to nZVI with initial rate = 64 mg $g^{-1}$ $min^{-1}$. The likely mechanism for observed reduction in $q_e$ is the blocking of active sorption sites on the nZVI surface by chitosan, which decreases the interaction between nZVI and phosphate anions. However, because the chitosan is positively charged in acidic medium, it likely improves the initial adsorption of phosphate anions to the nZVI surface.

### 3.3. Phosphorus adsorption isotherms

To assess the adsorption behavior of nZVI and CS-nZVI preparations, the experimental adsorption results were fitted using the Freundlich (Eq. (8)) and Langmuir (Eq. (9)) isotherm equations. The linear forms of the Freundlich and Langmuir models are presented in Eqs. (10) and (11).

$$q_e = k_f C_e^{1/n} \tag{8}$$

$$q_e = \frac{q_m K_L C_e}{1 + K_L C_e} \tag{9}$$

$$\log q_e = \log k_f + \frac{1}{n}\log C_e \tag{10}$$

$$\frac{C_e}{q_e} = \frac{1}{q_m K_L} + \frac{1}{q_m} C_e \tag{11}$$

where $q_e$ is the adsorbent capacity at equilibrium (mg/g); $C_e$ is the equilibrium concentration of phosphorus in solution (mg/L); $q_m$ is the Langmuir theoretical maximum adsorption capacity (mg/g), $k_f$ and $n$ are Freundlich constants and $K_L$ is Langmuir constant (L/mg). The Langmuir isotherm model assumes an adsorption monolayer that contains a finite number of homogeneous adsorption sites while the Freundlich isotherm assumes heterogeneous surface energies [27].

The experimental data fitted with the Freundlich and Langmuir models are shown in Figs. 8–11 and the parameters of the two models are summarized in Table 2.

For removal using nZVI, the experimental data were well represented by both Freundlich and Langmuir

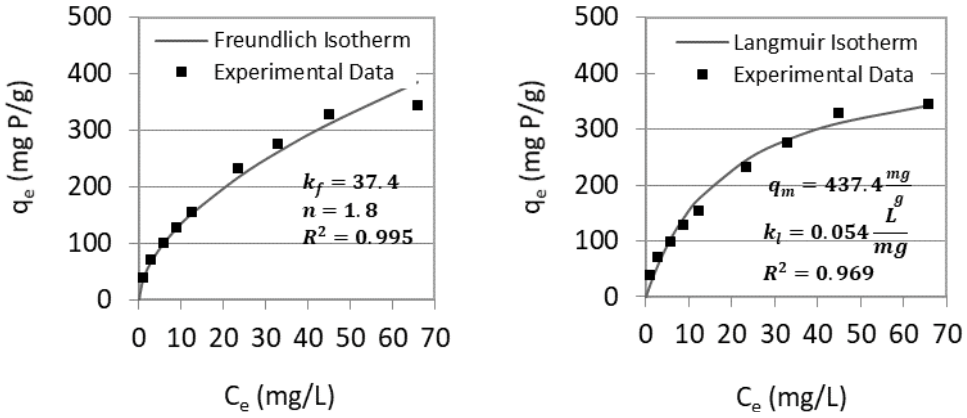


Fig. 8. Freundlich and Langmuir representation of phosphorus adsorption onto nZVI particles at pH 5.

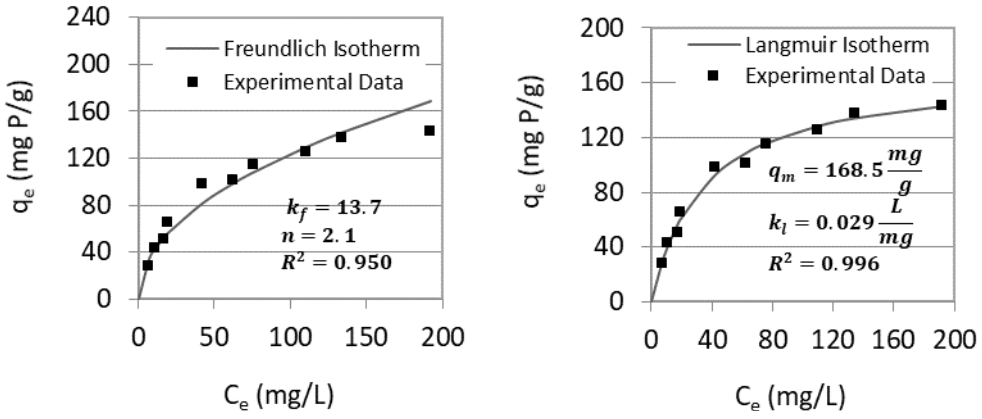


Fig. 9. Freundlich and Langmuir representation of phosphorus adsorption onto nZVI particles at pH 7.

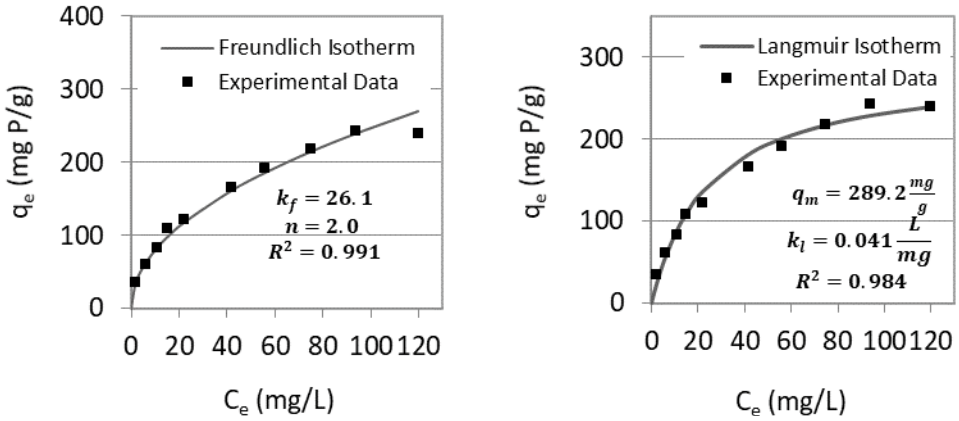


Fig. 10. Freundlich and Langmuir representation of phosphorus adsorption onto CS-nZVI particles at pH 5.

isotherms at both pH 5 and pH 7, with ($R^2$ > 0.95). The Langmuir theoretical maximum adsorption capacity ($q_m$) was 437 mg P/g nZVI at pH 5 compared to 169 mg P/g nZVI at pH 7 (Figs. 7 and 8). The adsorption capacities estimated from the isotherm experiments are consistent with those obtained from the kinetic studies ($q_m$ = 400 at pH 5 and $q_m$ = 130 at pH 7). In a previous study [16] phosphorus adsorption by nZVI was also well represented by both Langmuir and Freundlich models with $q_m$ = 246 mg/g at pH 5, which is much lower than the results reported in this study ($q_m$ = 437 mg/g).

Similarly for CS-nZVI, the experimental data were well represented by Freundlich and Langmuir isotherms at both pH 5 and 7 ($R^2$ > 0.92). The Langmuir theoretical maximum

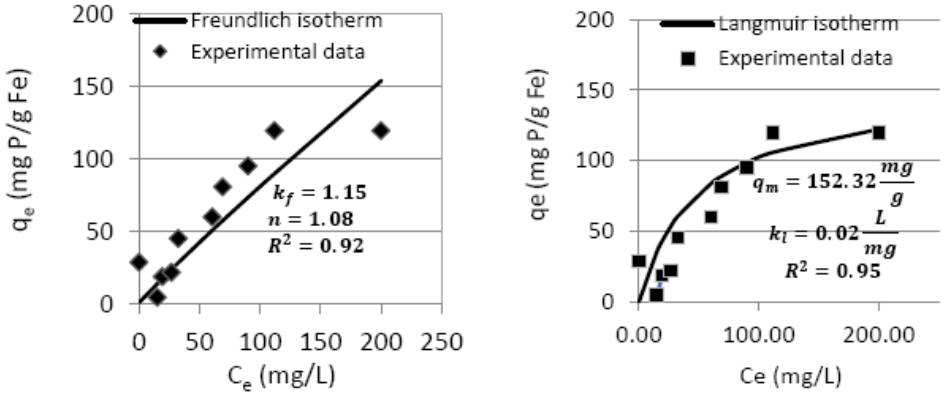


Fig. 11. Freundlich and Langmuir representation of phosphorus adsorption onto CS-nZVI particles at pH 7.

Table 2
Parameters for Freundlich and Langmuir isotherms

| Adsorbent | Solution | pH | Freundlich isotherm | | | Langmuir isotherm | | |
|---|---|---|---|---|---|---|---|---|
| | | | $k_f$ | $n$ | $R^2$ | $q_m$ (mg/g) | $k_l$ (L/mg) | $R^2$ |
| nZVI | $PO_4^{3-}$, solution | 5 | 37.4 | 1.8 | 0.995 | 437.4 | 0.054 | 0.969 |
| | | 7 | 13.7 | 2.1 | 0.950 | 168.5 | 0.029 | 0.996 |
| CS-nZVI | $PO_4^{3-}$, solution | 5 | 26.1 | 2.0 | 0.991 | 289.2 | 0.041 | 0.984 |
| | | 7 | 1.15 | 1.08 | 0.920 | 152.32 | 0.02 | 0.95 |
| nZVI | Mixture of $PO_4^{3-}$, $Cl^-$, $SO_4^{2-}$, $NO_3^-$ | 5 | 35 | 1.8 | 0.914 | 453.3 | 0.044 | 0.975 |
| | | 7 | 1.1 | 2.5 | 0.931 | 182.2 | 0.024 | 0.978 |

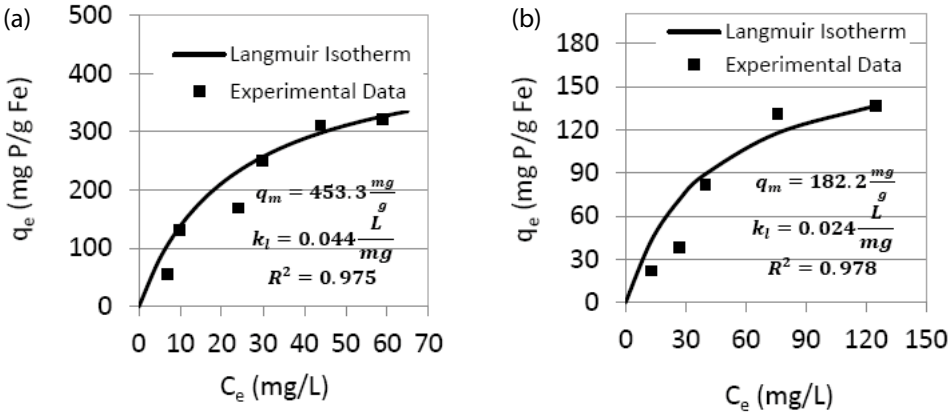


Fig. 12. Comparison of phosphorus adsorption capacities in the presence of competing for anions ($Cl^-$, $NO_3^-$, $SO_4^{2-}$) at (a) pH 5 and (b) pH 7.

adsorption capacity ($q_m$) was 289.2 mg P/g CS-nZVI at pH 5 while at pH 7 it was 152.3 mg P/g (Figs. 9 and 10). Upon comparing $q_m$ for nZVI and CS-nZVI at pH 5 we observe a decrease in adsorption capacity from 437.4 mg/g to 289.2 mg/g respectively. However, the adsorption capacities at pH 7 did not change drastically between nZVI and CS-nZVI (168.5 mg/g for nZVI compared to 152.3 mg/g for CS-nZVI). The trends for adsorption isotherms for both nZVI and CS-nZVI are similar to trends observed in $q_e$ values in kinetic experiments. The variation in the applicability of the different adsorption isotherm models may be due to the involvement of multi-removal mechanisms, including adsorption, ion exchange and precipitation.

The differences in phosphorus adsorption capacities from solutions containing phosphorus alone and from solutions containing phosphorus and other potentially competing anions ($Cl^-$, $SO_4^{2-}$, $NO_3^-$) were assessed using nZVI only and the results are shown in Fig. 12. The data show that the adsorption capacities from the mixtures at both pH 5 and 7 were low at the lower equilibrium concentrations compared

to the capacities at the higher adsorption concentrations. However, available data suggest that at the higher equilibrium concentrations, the adsorption capacities from the mixtures of anions were consistent with those obtained for the phosphorus solutions alone. Unfortunately, the available data are not enough to provide a clear explanation of the observed differences, but the results indicate an impact on competing anions at lower equilibrium concentrations.

Previous studies have also demonstrated that adsorption of phosphorus by nZVI was well represented by both Langmuir and Freundlich models and the maximum adsorption capacity reported was 246 mg/g [16]. In comparison, in this study significantly higher removal of phosphorus was observed with the maximum adsorption capacity of 437 mg/g in deionized water.

## 4. Conclusion

This study showed that both nZVI and CS-nZVI effectively removed phosphorus from solution and achieved relatively high adsorption capacities. To our knowledge, this is the first study that highlights the performance of chitosan-coated nZVI on phosphate removal. Furthermore, the presence of competing for anions ($Cl^-$, $SO_4^{2-}$, $NO_3^-$) did not significantly affect nZVI phosphorus adsorption kinetics nor adsorption capacities. The phosphorus adsorption capacities were pH-dependent for both types of adsorbents, nZVI is and CS-nZVI ($q_m$ = 400 mg/g at pH 5 and 130 mg/g at pH 7 for nZVI and $q_m$ = 238 mg/g at pH 5 and 118 mg/g at pH 7 for CS-nZVI). The phosphate removal capacity by nZVI (437 mg/g at pH 5) reported in this study is superior to those reported previously in the literature [18]. The addition of chitosan significantly reduced the adsorption capacity of nZVI at both pH 5 and pH 7, possibly due to coating the active sorption sites. The experimental data for both nZVI is and CS-nZVI were well represented by both Langmuir and Freundlich isotherm models at pH 5 and 7. Furthermore, the adsorption kinetics followed pseudo-second-order kinetics, with higher initial adsorption rates at pH 5. The results from the study suggest that nZVI is a promising material for the removal of phosphorus from water.

## References


[1] W. Schipper, Phosphorus: too big to fail, Eur. J. Inorg. Chem., 10 (2014) 1567–1571.

[2] I. Ali, V.K. Gupta, Advances in water treatment by adsorption technology, Nat. Protoc., 1 (2007) 2661–2667.

[3] J. Peter, Phosphorus Adsorption through Engineered Biochars Produced from Local Waste Products, Civil and Environmental Engineering Department, University of Dayton, Ohio, 2016. Available at: https://ecommons.udayton.edu/uhp_theses/141

[4] R. Xie, Y. Chen, T. Cheng, Y. Lai, W. Jiang, Z. Yang, Study on an effective industrial waste-based adsorbent for the adsorptive removal of phosphorus from wastewater: equilibrium and kinetics studies, Water Sci. Technol., 73 (2016) 1891–1900.

[5] C. Jiang, L. Jia, Y. He, B. Zhang, G. Kirumba, J. Xie, Adsorptive removal of phosphorus from aqueous solution using sponge iron and zeolite, J. Colloid Interface Sci., 402 (2013) 246–252.

[6] C. Jiang, L. Jia, B. Zhang, Y. He, G. Kirumba, Comparison of quartz sand, anthracite, shale and biological ceramsite for adsorptive removal of phosphorus from aqueous solution, J. Environ. Sci., 26 (2014) 466–477.

[7] S. Moharami, M. Jalali, Use of modified clays for removal of phosphorus from aqueous solutions, Environ. Monit. Assess., 187 (2015), doi: 10.1007/s10661–015–4854–2.

[8] A.M. Shanableh, M.M. Elsergany, Removal of phosphate from water using six Al-, Fe-, and Al-Fe-modified bentonite adsorbents, J. Environ. Sci. Health. Part A, 48 (2013) 223–231.

[9] A. Shanableh, G. Enshasi, M. Elsergany, Phosphorous adsorption using $Al^{3+}$/$Fe^{3+}$-modified bentonite adsorbents—effect of $Al^{3+}$ and $Fe^{3+}$ combinations, Desal. Wat. Treat., 57 (2016) 15628–15634.

[10] M. Shanableh, A. Elsergany, Phosphorus Removal using Al-modified Bentonite Clay–effect of Particle Size, 2012 Asia Pacific Conference on Environmental Science, Advances in Biomedical Engineering, Kuala Lumpur, Malaysia, 6 (2012) 323–329.

[11] P. Kwangyong, L. Warangkana, J. Seokwon, L.K. Young, Adsorptive Removal of Phosphate from Wastewater using Mesoporous Titanium Oxide, The 2016 World Congress on Advances in Civil, Environmental, and Materials Research (ACEM16), Jeju Island, Korea, 2016.

[12] J.W. Choi, S.Y. Lee, K.Y. Park, K.B. Lee, D.J. Kim, S.H. Lee, Investigation of phosphorus removal from wastewater through ion exchange of mesostructure based on inorganic material, Desalination, 266 (2011) 281–285.

[13] P.G. Tratnyek, R.L. Johnson, Nanotechnologies for environmental cleanup, Nano Today, 1 (2006) 44–48.

[14] N.C. Mueller, J. Braun, J. Bruns, M. Černík, P. Rissing, D. Rickerby, B. Nowack, Application of nanoscale zero valent iron (nZVI) for groundwater remediation in Europe, Environ. Sci. Pollut. Res., 19 (2012) 550–558.

[15] R. Mukherjee, R. Kumar, A. Sinha, Y. Lama, A.K. Saha, A review on synthesis, characterization, and applications of nano zero-valent iron (nZVI) for environmental remediation, Crit. Rev. Env. Sci. Technol., 46 (2016) 443–466.

[16] W.X. Zhang, D.W. Elliott, Applications of iron nanoparticles for groundwater remediation, Rem. J. Environ. Cleanup Costs Technol. Tech., (2006), https://doi.org/10.1002/rem.20078.

[17] N.C. Mueller, B. Nowack, Nanoparticles for remediation: solving big problems with little particles, Elements, 6 (2010) 395–400.

[18] Z. Wen, Y. Zhang, C. Dai, Removal of phosphate from aqueous solution using nanoscale zerovalent iron (nZVI), Colloids Surf., A, 457 (2014) 433–440.

[19] S. Wu, D. Shen, Y. Ding, A. Qiu, M. Yang, Q. Zheng, Phosphate removal from aqueous solutions by nanoscale zero-valent iron, Environ. Technol., 34 (2013) 2663–2669.

[20] T.Y. Liu, L. Zhao, Z.L. Wang, Removal of hexavalent chromium from wastewater by $Fe^0$-nanoparticles-chitosan composite beads: characterization, kinetics, and thermodynamics, Water Sci. Technol., 66 (2012) 1044–1051.

[21] B. Geng, Z. Jin, T. Li, X. Qi, Preparation of chitosan-stabilized $Fe^0$ nanoparticles for removal of hexavalent chromium in water, Sci. Total Environ., 407 (2009) 4994–5000.

[22] B. Geng, Z. Jin, T. Li, X. Qi, Kinetics of hexavalent chromium removal from water by chitosan-$Fe^0$ nanoparticles, Chemosphere, 75 (2009) 825–830.

[23] G. Unsoy, S. Yalcin, R. Khodadust, G. Gunduz, U. Gunduz, Synthesis optimization and characterization of chitosan-coated iron oxide nanoparticles produced for biomedical applications, J. Nanopart. Res., 14 (2012) 1–13.

[24] T. Almeelbi, A. Bezbaruah, Aqueous phosphate removal using nanoscale zero-valent iron, J. Nanopart. Res., (2014) 197–210, doi: 10.1007/s11051–012–0900-y.

[25] S. Nagoya, S. Nakamichi, Y. Kawase, Mechanisms of phosphate removal from aqueous solution by zero-valent iron: a novel kinetic model for electrostatic adsorption, surface complexation and precipitation of phosphate under oxic conditions, Sep. Purif. Technol., 218 (2019) 120–129.

[26] D.-G. Kim, Y.-H. Hwang, H.-S. Shin, S.-O. Ko, Kinetics of nitrate adsorption and reduction by nano-scale zero-valent iron (nZVI): Effect of ionic strength and initial pH, KSCE J. Civ. Eng., 20 (2016) 175–187.

[27] G. Vijayakumar, R. Tamilarasan, M. Dharmendirakumar, Adsorption, kinetic, equilibrium and thermodynamic studies on the removal of basic dye Rhodamine-B from aqueous solution by the use of natural adsorbent perlite, J. Mater. Environ. Sci., 3 (2012) 157–170.